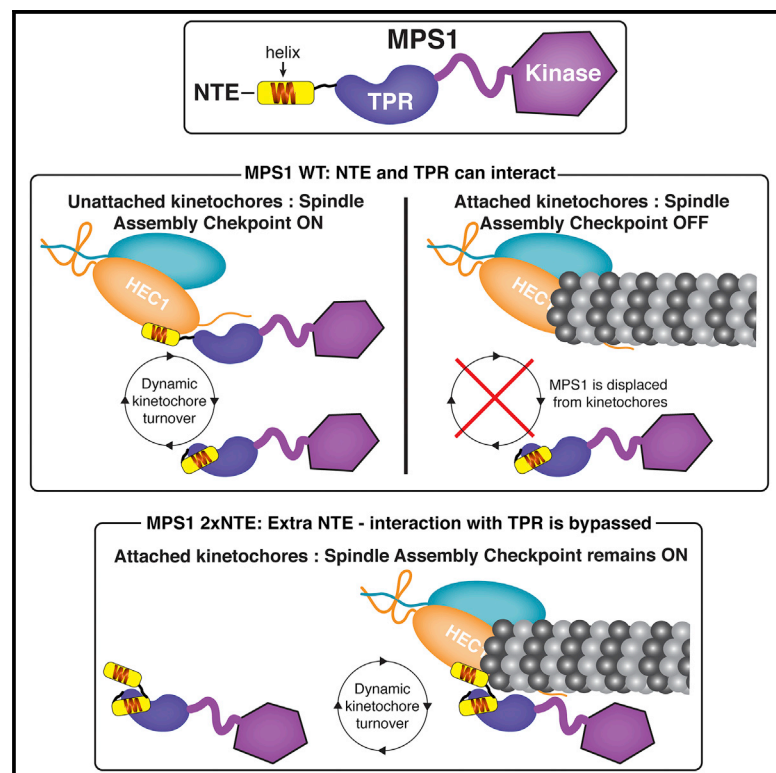


Interactions between N-terminal Modules in MPS1 Enable Spindle Checkpoint Silencing

Graphical Abstract



Authors

Spyridon T. Pachis, Yoshitaka Hiruma, Eelco C. Tromer, Anastassis Perrakis, Geert J.P.L. Kops

Correspondence

g.kops@hubrecht.eu

In Brief

Pachis et al. show that proper binding dynamics of the spindle checkpoint kinase MPS1 to kinetochores are ensured by regulated intramolecular interactions. Perturbing these interactions can lead to inefficient displacement of MPS1 upon microtubule attachment and defects in inactivating the spindle assembly checkpoint, which is necessary for timely chromosome segregation.

Highlights

- MPS1 kinase localizes to kinetochores via a helical fragment in its NTE module
- The NTE can interact with the neighboring TPR domain
- The NTE-TPR interaction regulates the binding of MPS1 to kinetochores
- Disrupting this interaction perturbs SAC silencing without affecting MT attachments



Interactions between N-terminal Modules in MPS1 Enable Spindle Checkpoint Silencing

Spyridon T. Pachis,¹ Yoshitaka Hiruma,² Eelco C. Tromer,³ Anastassis Perrakis,² and Geert J.P.L. Kops^{1,4,*}

¹Onco Institute, Hubrecht Institute-KNAW and University Medical Center Utrecht, Utrecht, 3584 CT, the Netherlands

²Department of Biochemistry, the Netherlands Cancer Institute, Amsterdam, 1066 CX, the Netherlands

³Department of Biochemistry, University of Cambridge, Cambridge CB2 1QW, UK

⁴Lead Contact

*Correspondence: g.kops@hubrecht.eu

<https://doi.org/10.1016/j.celrep.2019.01.017>

SUMMARY

Faithful chromosome segregation relies on the ability of the spindle assembly checkpoint (SAC) to delay anaphase onset until chromosomes are attached to the mitotic spindle via their kinetochores. MPS1 kinase is recruited to kinetochores to initiate SAC signaling and is removed from kinetochores once stable microtubule attachments have been formed to allow normal mitotic progression. Here, we show that a helical fragment within the kinetochore-targeting N-terminal extension (NTE) module of MPS1 is required for interactions with kinetochores and forms intramolecular interactions with its adjacent tetratricopeptide repeat (TPR) domain. Bypassing this NTE-TPR interaction results in high MPS1 levels at kinetochores due to loss of regulatory input into MPS1 localization, inefficient MPS1 delocalization upon microtubule attachment, and SAC silencing defects. These results show that SAC responsiveness to attachments relies on regulated intramolecular interactions in MPS1 and highlight the sensitivity of mitosis to perturbations in the dynamics of the MPS1-NDC80-C interactions.

INTRODUCTION

Genomic stability is a key feature of cellular homeostasis, and error-free chromosome segregation during mitosis is crucial for maintaining it (Ricke and van Deursen, 2013). The spindle assembly checkpoint (SAC) safeguards this process by prohibiting cells from separating their duplicated chromosomes in anaphase until all of them are properly attached to microtubules of the mitotic spindle (Etemad and Kops, 2016; London and Biggins, 2014a). The SAC is satisfied only when all chromosomes have made stable, bioriented attachments, a state in which each of the two sister chromatids is attached exclusively to microtubules emanating from opposing spindle poles. Any other attachment conformations are sensed and destabilized by the error correction machinery (Carmena et al., 2012).

Unattached kinetochores elicit a SAC response by the hierarchical recruitment of SAC components, including BUBs (BUB1,

BUB3, and BUBR1) and MADs (MAD1 and MAD2). Eventually, this leads to the production of a diffusible anaphase inhibitor known as the mitotic checkpoint complex (MCC) (Chao et al., 2012; Hardwick et al., 2000; Musacchio, 2015; Sudakin et al., 2001). The MCC is responsible for blocking activation of the anaphase promoting complex/cyclosome (APC/C)^{CDC20} complex, whose function is to promote the transition to anaphase. SAC signaling is locally silenced when microtubules form stable attachments to a kinetochore, ultimately followed by full SAC satisfaction (MCC disassembly) when all chromosomes have achieved stable attachments (Etemad and Kops, 2016; Funabiki and Wynne, 2013; Kops and Shah, 2012; Sacristan and Kops, 2015).

Monopolar spindle 1 (MPS1) kinase is the major orchestrator of SAC signaling (Pachis and Kops, 2018). It is recruited to unattached kinetochores, where it autoactivates and subsequently phosphorylates its kinetochore substrates to recruit downstream SAC components and enable MCC production (Jelluma et al., 2008a; Kang et al., 2007; Lan and Cleveland, 2010; London and Biggins, 2014a; Mattison et al., 2007; Stucke et al., 2002). MPS1 phosphorylates multiple residues on at least three proteins involved in the recruitment cascade (Knl1, Bub1, and Mad1) (Faesen et al., 2017; Ji et al., 2017; London and Biggins, 2014b; London et al., 2012; Shepperd et al., 2012; Yamagishi et al., 2012); subsequently, it may directly affect MCC stability and its binding to the APC/C (Zich et al., 2012). Besides its role in the SAC, MPS1 is involved in the regulation of chromosome biorientation (Jelluma et al., 2008b; Maciejowski et al., 2017; Maure et al., 2007; Saurin et al., 2011) and in the expansion of kinetochores in early prometaphase (Rodriguez-Rodriguez et al., 2018; Sacristan et al., 2018).

MPS1 contains in its N terminus an N-terminal extension (NTE) sequence module followed by a tetratricopeptide repeat (TPR) domain. Although the NTE provides the predominant localization signal, both modules are involved in MPS1's ability to localize to kinetochores via direct binding to members of the NDC80 complex (Araki et al., 2010; Hiruma et al., 2015; Ji et al., 2015; Kemmler et al., 2009; Nijenhuis et al., 2013; Stucke et al., 2004). The mitotic kinase Aurora B plays an important role in promoting MPS1 kinetochore localization (Santaguida et al., 2011; Saurin et al., 2011), at least partly by alleviating an inhibitory effect that the TPR imposes on kinetochore binding via the NTE (Nijenhuis et al., 2013). MPS1 signaling at kinetochores diminishes upon microtubule binding due to competition between MPS1



and microtubules for binding to the NDC80 complex (Hiruma et al., 2015; Ji et al., 2015). Aided by high turnover of kinetochore MPS1 (Howell et al., 2004; Jelluma et al., 2010), this results in reduced ability of MPS1 molecules to re-bind kinetochores once they are occupied by microtubules. In this way, SAC signaling is disrupted at its most upstream point—a mechanism that, alongside other ways of silencing the SAC, eventually causes full SAC inactivation and anaphase onset (Aravamudan et al., 2015; Espert et al., 2014; Etemad and Kops, 2016; Eytan et al., 2014; Foster and Morgan, 2012; Gassmann et al., 2010; Howell et al., 2001; Kops and Shah, 2012; Kruse et al., 2013; London et al., 2012; Mische et al., 2008; Moura et al., 2017; Nijenhuis et al., 2014; Rosenberg et al., 2011; Uzunova et al., 2012; Wang et al., 2014; Westhorpe et al., 2011; Ye et al., 2015).

The localization of MPS1 to kinetochores and the regulation thereof are crucial for the SAC, yet much is still unknown about the mechanisms that dictate it. Here, we set out to examine the potential interplay among the different N-terminal regions in MPS1 and determine how they regulate its kinetochore levels. We report the presence of a helical fragment in the NTE of MPS1 that is important for its kinetochore localization, and we detect a direct intramolecular interaction between the NTE and the TPR modules of MPS1. This interaction dampens MPS1 kinetochore binding, which we show is important for efficient SAC silencing.

RESULTS

A Short Helical Fragment in the NTE Is Important for MPS1 Kinetochore Localization

Previous work determined the crystallographic structure of Mps1⁶²⁻²³⁹, allowing the identification of the TPR domain structure (PDB: 4B94, 4H7X, 4H7Y) (Nijenhuis et al., 2013; Thebaud et al., 2012). The last 40 residues in that structure were not visible in the electron density maps and are thus presumably flexible or disordered. To gain more insight into the structure and properties of MPS1's N-terminal kinetochore localization modules, we performed nuclear magnetic resonance (NMR) analysis on MPS1¹⁻²³⁹, containing both the NTE module (which was not present in the crystallized protein) and the C-terminal extension (CTE) of the TPR domain (the last 40 residues that were not modeled). 87% of the residues in MPS1¹⁻²³⁹ were successfully assigned to their corresponding NMR chemical shifts (Figure S2). From the assignment, it was evident that the NTE had chemical shifts characteristic of a flexible conformation. To further investigate that, we used the TALOS software (Shen and Bax, 2013) to predict secondary structure elements of the NTE based on the NMR spectra. TALOS confirmed that the NTE likely assumes a flexible conformation but also predicted (albeit with a low score) that residues 14–23 have the propensity to form a helix (Figure 1A). Alignment of animal NTE sequences shows substantial divergence but relatively high conservation in key residues of the predicted helix (Figure S1A). To examine the importance of this potential helical fragment, we designed a helix-disrupting point mutation in the NTE by substituting an asparagine residue in the middle for a proline residue (Figures 1A and 1B) and assessed the ability

of MPS1 to localize to kinetochores of prometaphase cells treated with MPS1 inhibitor (to exclude potential secondary effects on localization via altered MPS1 activity) (Jelluma et al., 2010). MPS1 carrying the N18P mutation showed greatly reduced kinetochore levels in cells treated with nocodazole (Figures 1C and 1D), without affecting protein stability (Figure S1B). The low kinetochore levels of MPS1^{N18P} were similar to those of MPS1^{Δ60}, a mutant in which the entire NTE is removed (Figures 1C and 1D) (Dou et al., 2015; Nijenhuis et al., 2013). Combining the N18P substitution with a deletion of the TPR domain (MPS1^{N18P-ΔTPR}) abolished MPS1 kinetochore binding to a similar extent as deleting the entire NTE-TPR module (MPS1^{Δ200}) (Figures 1C and 1D) (Nijenhuis et al., 2013). We next measured mitotic delays in cells treated with nocodazole and a low dose of the MPS1 inhibitor Cpd-5 (25 nM) (Koch et al., 2016) to uncover potential subtle differences in SAC strength among the different cell lines. In agreement with compromised localization, cells expressing MPS1^{N18P} and MPS1^{N18P-ΔTPR} were impaired in maintaining a mitotic arrest when treated with nocodazole (Figure 1E). Altogether, these data are consistent with a role for an N-terminal α helix in enabling the interaction between the NTE and the NDC80-C.

The TPR Domain and NTE of MPS1 Interact

Our previous work suggested that regulation of MPS1 localization involves release of an inhibitory effect of the TPR domain on the NTE (Nijenhuis et al., 2013). To examine whether this could be via direct interactions between the two modules, we first assigned chemical shifts to MPS1⁶²⁻²³⁹ (Figure 2A). We then compared the ¹H, ¹⁵N heteronuclear single-quantum correlation (HSQC) spectra of MPS1¹⁻²³⁹ and MPS1⁶²⁻²³⁹ to measure chemical shift perturbations (CSPs) (Figure 2B), which we mapped onto the sequence and crystal structure of the TPR domain (Figures 2C and 2D). The largest CSPs, indicative of interaction sites with the NTE, were observed at the convex outer surface of the TPR, mostly at the two N-terminal α helices (63–73 and 82–98) and considerably less so on the rest of the outer surface. Few CSPs were measured at the concave inner surface of the TPR. Surface conservation analysis of the TPR domain shows little overlap between the more conserved residues and those that display the largest CSPs in the NMR experiments (Figure 2E). This is not surprising, because residues that maintain the TPR fold are expected to be more conserved than those interacting with a divergent, largely unstructured NTE. To assess the contribution of electrostatic interactions to the interaction of the NTE with the TPR, we measured ¹H, ¹⁵N HSQC spectra of the two MPS1 variants upon titration of KCl (Figures S3A and S3C). Whereas the chemical shifts of MPS1⁶²⁻²³⁹ showed relatively small changes (Figures S3A and S3B), notable spectral perturbations were observed for MPS1¹⁻²³⁹ (Figures S3C and S3D), suggesting that the NTE-TPR interactions are largely electrostatic. The N-terminal region of the TPR domain on the convex outer surface, as well as the predicted helical residues in the NTE, showed relatively large CSPs upon KCl titration, confirming that these two regions are involved in the interaction (Figures S3E–S3G). These experiments suggest that the flexible NTE can interact with the proximal side of the convex outer surface of the TPR domain and that this depends on electrostatic interactions.

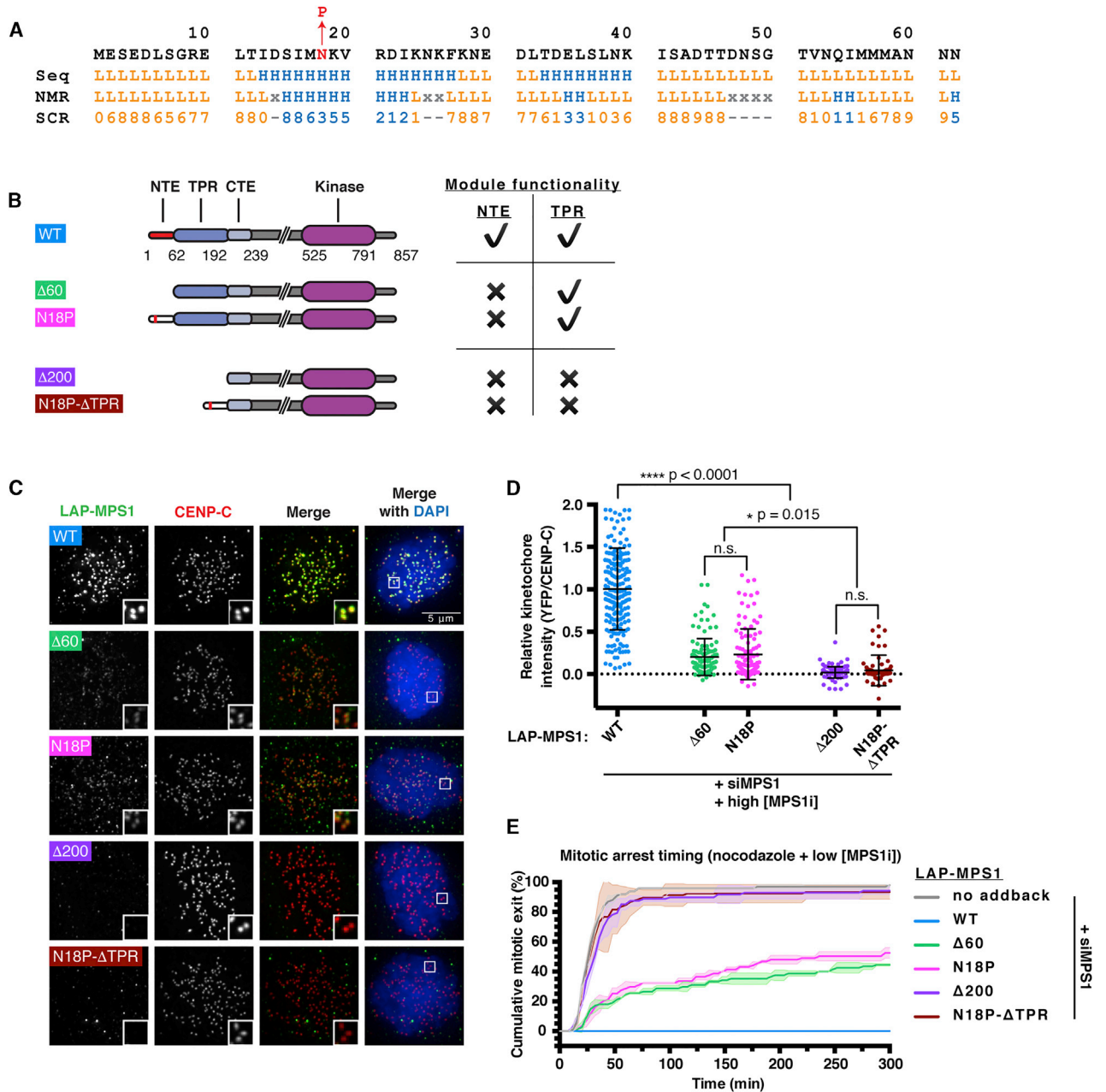


Figure 1. The NTE Contains a Short Helical Fragment that Is Important for MPS1 Kinetochore Localization

(A) Secondary structure prediction of the NTE. The “Seq” row shows the prediction based on the primary sequence, the “NMR” row shows the prediction based on the generated NMR spectra, and the “SCR” row is the confidence score per position for predictions based on NMR.

(B) Schematic representation and functional classification of the different MPS1 variants.

(C and D) Representative images (C) and quantification (D) of protein localization at kinetochores in nocodazole-treated and MPS1 inhibitor Cpd-5 (250 nM)-treated HeLa Flp-In cells transfected with MPS1 siRNA and expressing the indicated LAP-MPS1 variants. The graph shows the mean kinetochore intensity (\pm SD) normalized to the values of MPS1^{WT}. Each dot represents one cell, and all cells have been pooled from three independent experiments (WT, $n = 195$; Δ60, $n = 118$; N18P, $n = 111$; Δ200, $n = 100$; N18P-ΔTPR, $n = 65$). Asterisks indicate significance (one-way ANOVA followed by Tukey’s test).

(E) Time-lapse analysis of the duration of mitotic arrest in nocodazole-treated and Cpd-5 (25 nM)-treated HeLa Flp-In cells transfected with MPS1 siRNA and expressing the indicated LAP-MPS1 variants. The graph displays the mean values (\pm SD) from two independent experiments ($n = 75$ per condition).

See also Figure S1.

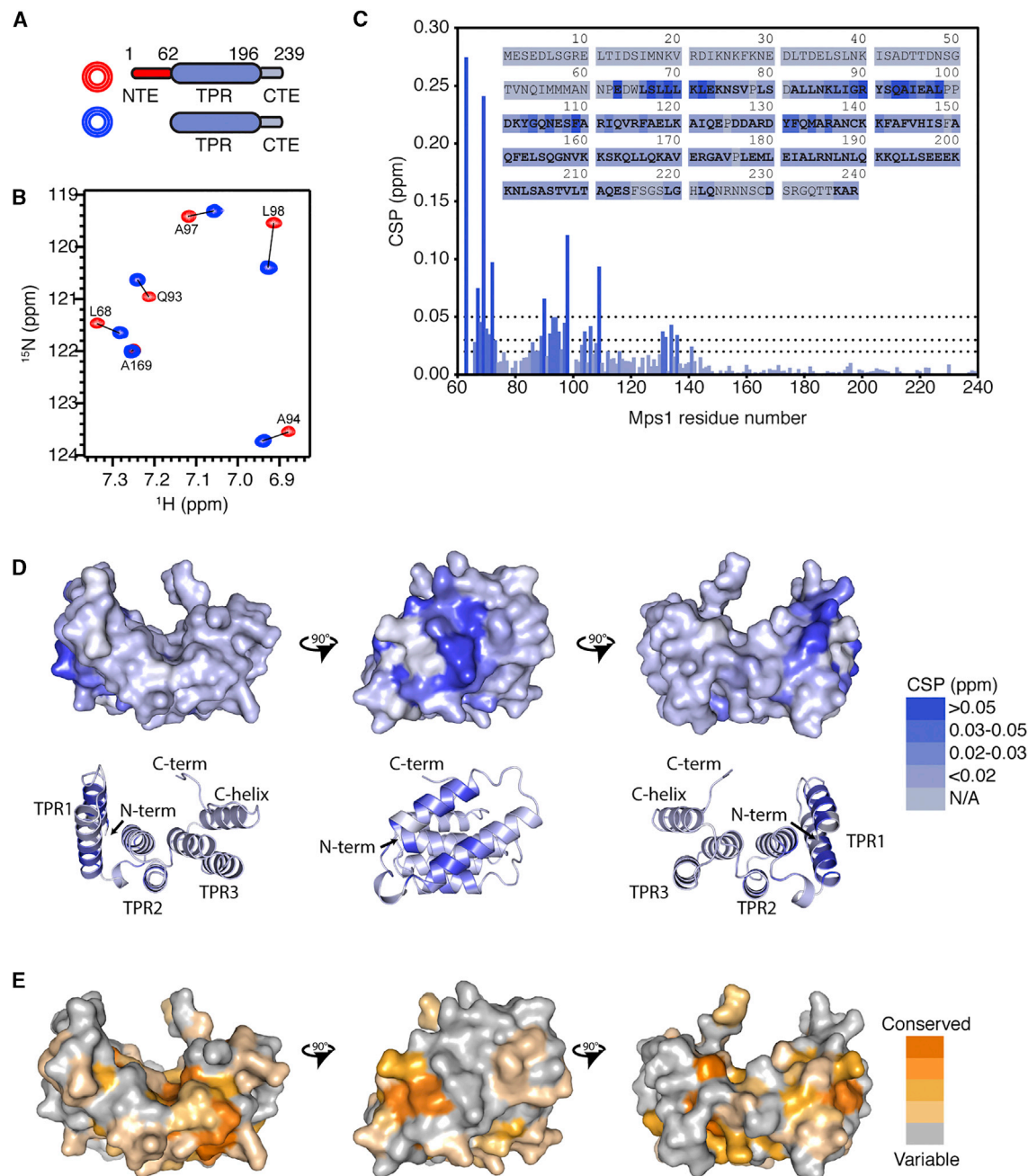


Figure 2. NMR of MPS1 N-terminal Fragments Uncovers NTE-TPR Interactions

(A) Schematic representation of the variants of MPS1 that were used.

(B) Examples of spectra showing residues in the TPR that are affected by the presence of the NTE (shifts from blue to red).

(C) Display of the chemical shift perturbations (CSPs) per residue in the sequence of the TPR-CTE region, color coded based on the CSP magnitude.

(D) Projection of the CSPs onto the crystal structure of the TPR domain (in 3 orientations) following the same color coding as in (C).

(E) Surface conservation of the TPR domain of MPS1, color coded per residue based on the sequence divergence in the species that were used (same 3 orientations as in D).

See also Figures S2 and S3.

Bypassing the NTE-TPR Interaction Leads to Constitutively Elevated Levels of MPS1 on Kinetochores

We next wished to examine the functional relevance of a regulated NTE-TPR interaction. Prior work showed that deletion of

the TPR domain or the NTE affected the ability of MPS1 to bind kinetochores (Dou et al., 2015; Nijenhuis et al., 2013), precluding the use of such approaches to disrupt the NTE-TPR interaction. We were also unable to identify specific residues in

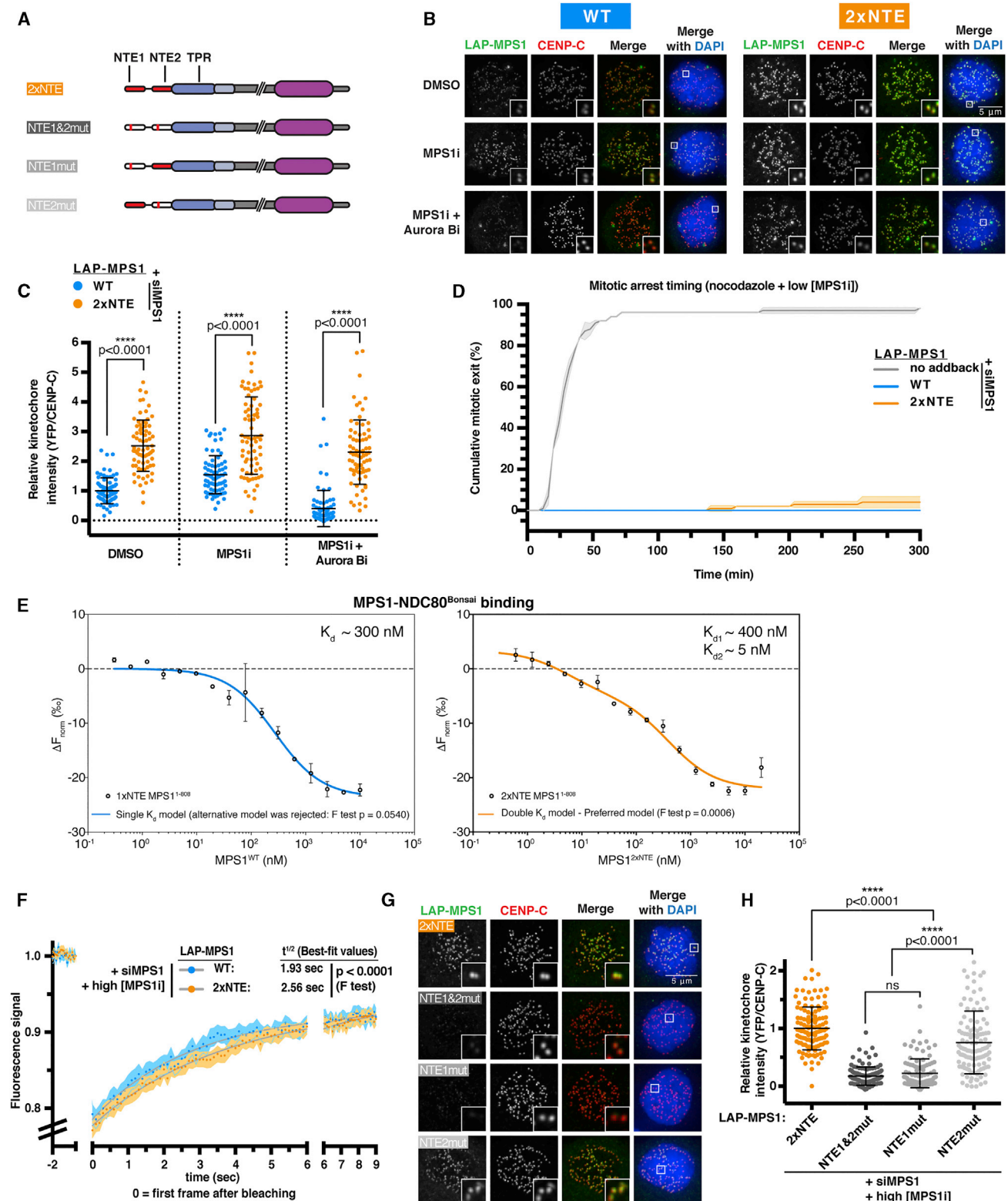


Figure 3. Bypassing the NTE-TPR Interaction Abolishes Kinase Regulation of MPS1 Kinetochore Localization

(A) Schematic representation of the MPS1 variants used.

(B and C) Representative images (B) and quantification (C) of protein levels at kinetochores in HeLa Flip-In cells transfected with MPS1 siRNA, expressing the indicated LAP-MPS1 variants and treated with nocodazole and the indicated inhibitors. The graph shows the mean kinetochore intensity (\pm SD) normalized to the (legend continued on next page)

NTE or TPR that affected NTE-TPR interaction without affecting their ability to bind kinetochores (data not shown). To bypass the NTE-TPR interaction without compromising the integrity of the NTE or TPR, we created MPS1^{2xNTE}, a version of MPS1 that contains an additional NTE fused to its N terminus (Figure 3A). As predicted, MPS1^{2xNTE} kinetochore levels were largely insensitive to inhibition of Aurora B kinase activity (Figures 3B and 3C). However, they were roughly two times higher than those of MPS1^{WT} and were additionally insensitive to inhibition of MPS1 activity, in contrast to MPS1^{WT} (Figures 3B and 3C). Enhanced levels of MPS1^{2xNTE} on kinetochores and insensitivity to MPS1 inhibition could not be explained by compromised kinase activity of MPS1^{2xNTE} (Hewitt et al., 2010; Jelluma et al., 2010; Kwiatkowski et al., 2010; Sliedrecht et al., 2010), because cells expressing this mutant were able to efficiently support the SAC in cells treated with nocodazole and a low dose of Cpd-5 (Figure 3D). These results indicate that the interaction between the NTE and the TPR domain of MPS1 is important for the regulation of MPS1 kinetochore levels and that Aurora B affects them, at least partly, through the regulation of that interaction.

The NTE-TPR Interaction Promotes MPS1 Release from Kinetochores

We next tried to understand the nature of the increased kinetochore localization of MPS1^{2xNTE} and its insensitivity to kinase regulation. Kinetochore levels of both MPS1^{WT} and MPS1^{2xNTE} in cells treated with nocodazole were diminished upon knock-down of endogenous HEC1 by small interfering RNA (siRNA), confirming that MPS1^{2xNTE} kinetochore binding depends on NDC80-C (Figures S4A and S4B). To examine whether the elevated kinetochore levels of MPS1^{2xNTE} are a result of a higher binding affinity between MPS1 and HEC1, we purified full-length recombinant MPS1 variants from insect cells and titrated them to a fixed concentration of fluorescently labeled NDC80-C^{Bonsai} (Ciferri et al., 2008) in microscale thermophoresis (MST) experiments. MPS1^{WT} binding to NDC80-C^{Bonsai} fit a model consistent with a single binding event with a K_d of ~300 nM (Figure 3E, left panel). However, the binding of MPS1^{2xNTE} to NDC80-C^{Bonsai} is best described by a model with two binding events: one with a K_d of ~400 nM and one with a K_d of ~5 nM (Figure 3E, right panel). Similar results were obtained when using shorter versions of MPS1 (1–377) (Figure S4C). The appearance of the higher-affin-

ity binding event is likely due to the added, unregulated NTE module.

We next performed fluorescence recovery after photobleaching (FRAP) analysis of fluorescent MPS1 variants at single-kinetochore pairs of cells that were arrested in nocodazole to determine whether differences in residence times contribute to the differences in kinetochore levels. We did so in the presence of MPS1 inhibitor (Cpd-5) to exclude activity-related effects on its residence time (Jelluma et al., 2010). Consistent with the presence of a higher-affinity binding site on MPS1^{2xNTE} for NDC80-C, MPS1^{2xNTE} displayed significantly reduced turnover on kinetochores compared to MPS1^{WT} (F test, $p < 0.0001$) with best-fit recovery half-times at 2.56 and 1.93 s, respectively (95% confidence intervals of half-time: wild-type (WT), 1.65–2.34 s; 2xNTE, 2.19–3.0 s) (Figure 3F).

To determine the contribution of each NTE to kinetochore binding, we first introduced the N18P mutation to disrupt the helical fragments present in both NTEs (MPS1^{NTE1&2mut}) (Figure 3A). This severely compromised the ability of MPS1 to localize to kinetochores (Figures 3G and 3H). Whereas mutation of only the TPR-proximal NTE (MPS1^{NTE2mut}) left localization of MPS1 largely unaffected, mutation of the apical NTE (MPS1^{NTE1mut}) strongly reduced localization to levels similar to those of MPS1^{NTE1&2mut} (Figures 3G and 3H). This observation argues that the increased levels of MPS1^{2xNTE} on kinetochores, as well as the higher binding affinity in the MST experiments, are mediated predominantly by the apical N-terminal NTE. Our data show that bypassing the NTE-TPR interaction removes kinase regulatory input into MPS1 localization and creates a higher-affinity binding site for NDC80-C, which in turn leads to higher residence time of MPS1 on kinetochores.

Bypassing the NTE-TPR Interaction Causes SAC Silencing Defects

Removal of active MPS1 from kinetochores is a crucial step for silencing the SAC in metaphase (Hiruma et al., 2015; Jelluma et al., 2010; Ji et al., 2015). Because kinetochore release of MPS1^{2xNTE} is compromised, we next examined whether removal of MPS1 from metaphase kinetochores was affected, by arresting cells with the proteasome inhibitor MG132. In contrast to MPS1^{WT}, MPS1^{2xNTE} displayed significant retention on metaphase kinetochores, at levels approximately half of those observed in nocodazole-treated cells expressing the mutant

values of MPS1^{WT} in DMSO. Each dot represents one cell, and cells have been pooled from four independent experiments (WT_DMSO, $n = 75$; 2xNTE_DMSO, $n = 72$; WT_cpd5, $n = 75$; 2xNTE_cpd5, $n = 75$; WT_cpd5+ZM447439, $n = 74$; 2xNTE_cpd5+ZM447439, $n = 75$). Asterisks indicate significance (one-way ANOVA followed by Tukey's test).

(D) Time-lapse analysis of the duration of mitotic arrest in nocodazole-treated and Cpd-5 (25 nM)-treated HeLa Flp-In cells transfected with MPS1 siRNA and expressing the indicated LAP-MPS1 variants. The graph displays the mean values (\pm SD) from three independent experiments ($n = 75$ for all conditions).

(E) MST binding graph generated by titrating MPS1^{WT} (left panel) or MPS1^{2xNTE} (right panel) to 50 nM of NDC80-C^{Bonsai}. One- or two-site binding curves were fitted, and an F test was performed to select a preferred model.

(F) Quantification of FRAP performed on individual kinetochore pairs of nocodazole-treated and Cpd-5 (250 nM)-treated HeLa Flp-In cells transfected with MPS1 siRNA and expressing the indicated LAP-MPS1 variants. The graph displays the mean fluorescence intensity (\pm SEM) from two independent experiments (WT, $n = 45$; 2xNTE, $n = 42$).

(G and H) Representative images (G) and quantification (H) of protein levels on kinetochores in nocodazole-treated and Cpd-5 (250 nM)-treated HeLa Flp-In cells transfected with MPS1 siRNA and expressing the indicated LAP-MPS1 variants. The graph shows the mean kinetochore intensity (\pm SD) normalized to the values of MPS1^{2xNTE}. Each dot represents one cell, and cells have been pooled from five independent experiments (2xNTE, $n = 123$; NTE1&2mut, $n = 117$; NTE1mut, $n = 98$; NTE2mut, $n = 119$). Asterisks indicate significance (one-way ANOVA followed by Tukey's test).

See also Figures S1 and S4.

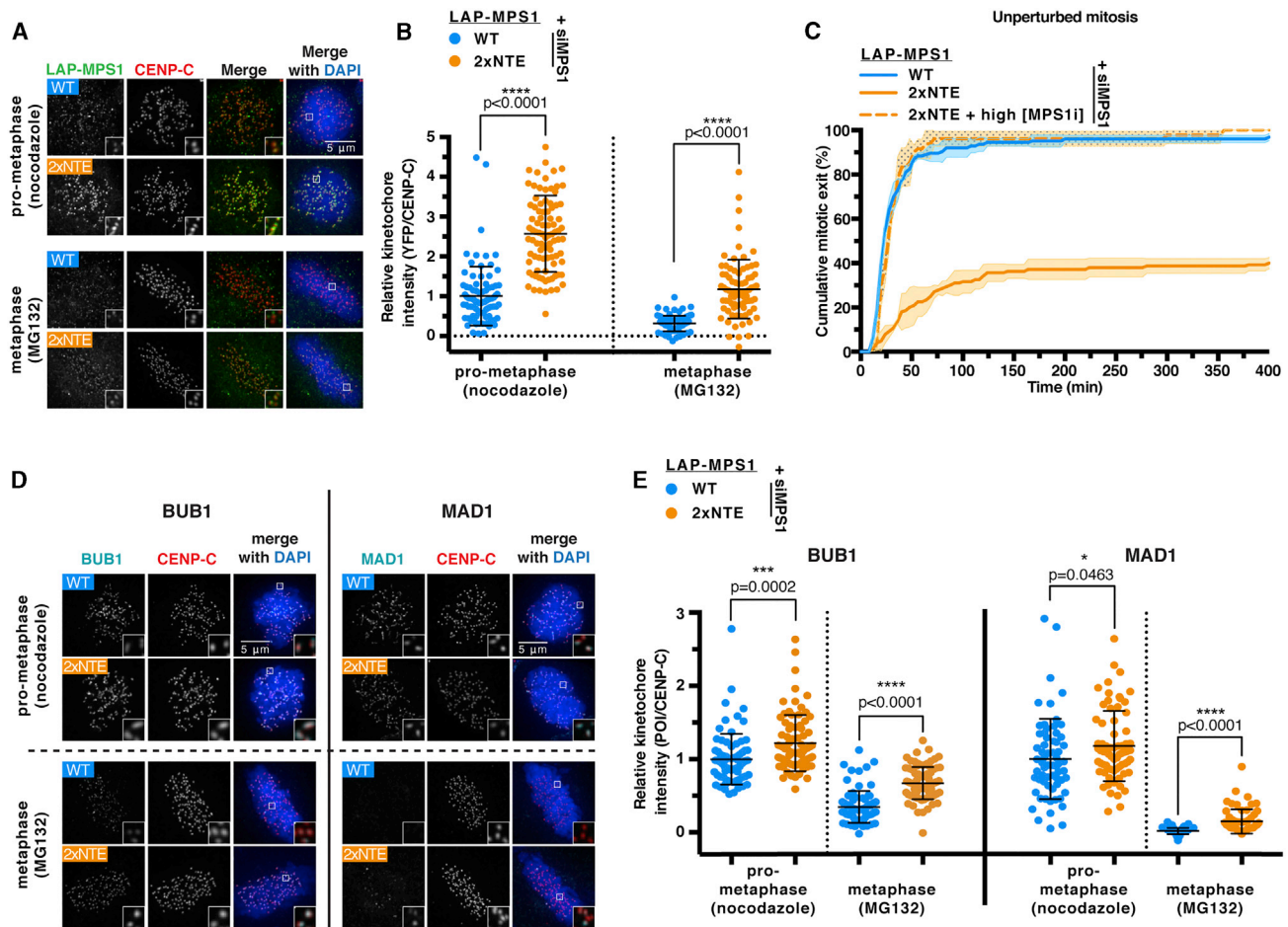


Figure 4. Bypassing the NTE-TPR Interaction Prevents SAC Silencing

(A and B) Representative images (A) and quantification (B) of nocodazole-treated or MG132-treated HeLa Flp-In cells transfected with MPS1 siRNA and expressing the indicated LAP-MPS1 variants. The graph displays the mean kinetochore intensity (\pm SD) normalized to the levels of MPS1^{WT} in prometaphase. Each dot represents one cell, and cells were pooled from four independent experiments (WT_noco, $n = 85$; 2xNTE_noco, $n = 90$; WT_MG132, $n = 81$; 2xNTE_MG132, $n = 80$). Asterisks indicate significance (Student's *t* test between the cell lines for each condition).

(C) Time-lapse analysis of the duration of DMSO-treated or MPS1 inhibitor Cpd-5 (250 nM)-treated HeLa Flp-In cells transfected with MPS1 siRNA and expressing the indicated LAP-MPS1 variants. The graph displays the mean values (\pm SD) from three independent experiments ($n = 100$ for all conditions).

(D and E) Representative images (D) and quantification (E) of the kinetochore levels of the indicated proteins in nocodazole-treated or MG132-treated HeLa Flp-In cells transfected with MPS1 siRNA and expressing the indicated LAP-MPS1 variants. The graph displays the mean kinetochore intensity (\pm SD) normalized to the levels of each protein in prometaphase MPS1^{WT}-expressing cells. For each protein examined, cells were pooled from three independent experiments and each dot represents one cell (BUB1, $n = 80$ for all conditions; MAD1, $n = 60$ for all conditions).

Asterisks indicate significance (Student's *t* test between different cell lines for each protein and condition).

See also Figure S4.

(Figures 4A and 4B). Time-lapse imaging of cells going through a round of unperturbed mitosis revealed that MPS1 retention on metaphase kinetochores was accompanied by a mitotic arrest. Whereas around 95% of MPS1^{WT}-expressing cells exited mitosis within 80 min from nuclear envelope breakdown (NEB), only 40% of MPS1^{2xNTE}-expressing cells managed to complete mitosis within 400 min (Figure 4C). The arrest was dependent on MPS1 activity (Figure 4C) and was consistently marked by elevated levels of KNL1-pT180, MAD1, and BUB1 on metaphase kinetochores. Although KNL1-pT180 and BUB1 were present at roughly 70% of the levels observed in nocodazole-treated cells, MAD1 was retained at only 15% (Figures 4D, 4E, S4D, and S4E).

We next examined whether weakened microtubule attachments due to the presence of elevated MPS1^{2xNTE} on metaphase kinetochores contributed to the mitotic arrest of the cells expressing this variant. Kinetochore-microtubule attachments were unaffected, as indicated by four observations. First, the time from NEB to metaphase was indistinguishable between cells expressing MPS1^{WT} and those expressing MPS1^{2xNTE} (Figures 5A and 5B). Second, the time from metaphase to cohesion loss by cohesion fatigue (Gorbsky, 2013) in MG132-treated cells was likewise similar (Figure 5C). Third, total levels of cold-stable tubulin of the mitotic spindle, as well as individual k-fiber intensities, were not substantially

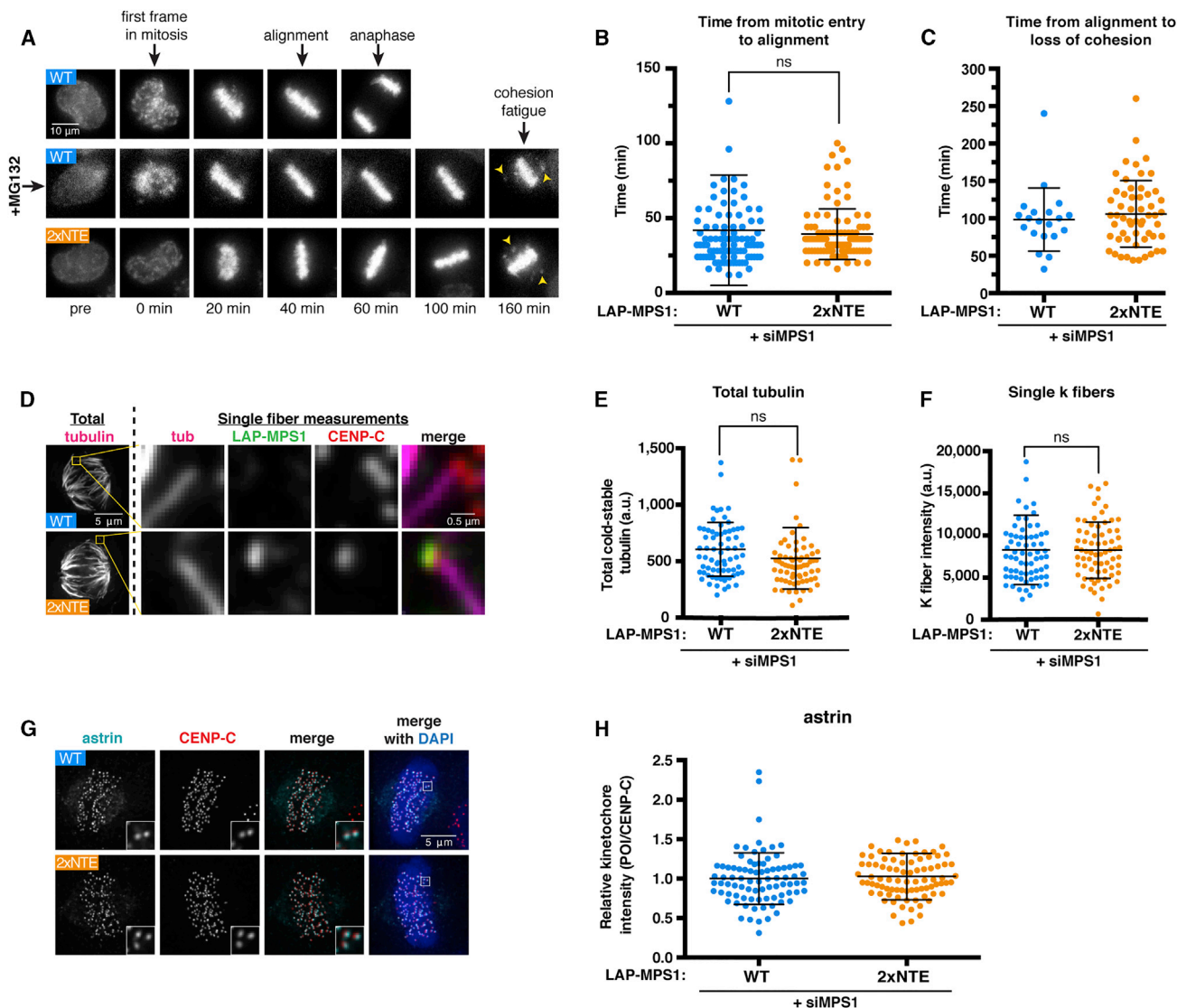


Figure 5. High Levels of MPS1 on Kinetochores in Metaphase Do Not Perturb Microtubule Attachments

(A–C) Representative stills (A) and quantifications (B and C) of time-lapse movies of HeLa Flp-In cells transfected with MPS1 siRNA and expressing the indicated LAP-MPS1 variants. Cells were incubated with SiR-DNA to visualize the chromatin and treated with either DMSO (WT and 2xNTE) or MG132 (WT only). Graphs in (B) and (C) display the absolute time in minutes (\pm SD). Each dot represents a cell, and cells were pooled from three independent experiments ($n = 95$ for both conditions) (B) or two independent experiments (WT, $n = 20$; 2xNTE, $n = 56$) (C). Student's t test showed no significant differences.

(D–F) Representative images (D) and quantifications (E and F) of cold-stable microtubules and of the indicated proteins on attached kinetochores in MG132-treated HeLa Flp-In cells transfected with MPS1 siRNA and expressing the indicated LAP-MPS1 variants. Graphs in (E) and (F) show quantification (a.u. \pm SD) of the total cold-stable tubulin levels (E) or of the intensity of individual k-fibers in each cell line (F). Each dot represents a cell, and cells were pooled from three independent experiments ($n = 70$ for all conditions and measurements). Student's t test showed no significant differences.

(G and H) Representative images (G) and quantification (H) of the kinetochore levels of astrin in MG132-treated HeLa Flp-In cells transfected with MPS1 siRNA and expressing the indicated LAP-MPS1 variants. The graph displays the mean kinetochore intensity (\pm SD) normalized to the levels of astrin in MPS1^{WT}-expressing cells. Cells were pooled from two independent experiments, and each dot represents one cell ($n = 85$ for both conditions).

See also Figure S4.

altered between cells expressing the two MPS1 variants (Figures 5D–5F), and no obvious correlation existed between the level of MPS1^{2xNTE} on single kinetochores and the k-fiber intensity (Figure S4F). Lastly, the levels of astrin, a marker of stable end-on attachments (Shrestha and Draviam, 2013), were not reduced on metaphase kinetochores of cells express-

ing MPS1^{2xNTE}, even though MPS1^{2xNTE} was still present there at high levels (Figures 5G and 5H). Altogether, these data show that bypassing the NTE-TPR interaction compromises the ability to silence the SAC by affecting the efficiency of MPS1 delocalization in metaphase without affecting microtubule attachments.

DISCUSSION

The work presented in this study suggests an additional mechanistic aspect of SAC silencing whereby regulated intramolecular interactions in MPS1 are important in removing it from kinetochores when microtubule attachments are formed. More specifically, we uncover a short helical fragment in the NTE of MPS1 that is important for interaction with its kinetochore receptor. We also report a direct electrostatically mediated interaction between the TPR domain and the NTE of MPS1. An MPS1 version designed to bypass this interaction is no longer regulated by Aurora B or itself and is inefficiently delocalized by microtubules in metaphase. A study using chemical crosslinking on recombinant MPS1 showed that crosslinks can be detected between the NTE and the TPR, confirming that the modules interact in full-length MPS1 (Combes et al., 2018).

We envision a model in which the NTE and TPR transiently interact, preventing efficient binding of MPS1 to kinetochores. The NTE-TPR interaction is diminished by Aurora B activity via unknown mechanisms, thereby enhancing affinity of MPS1 for kinetochores (Figure S5A). Once on kinetochores, the ability of the two modules to interact promotes MPS1 release and enables SAC silencing upon the formation of stable kinetochore-microtubule attachments (Figure S5B). The apical NTE, which we added in MPS1^{2xNTE}, is likely not able to interact with the TPR and is thus always available for interaction with kinetochores, leaving the Aurora B input mute. At the same time, the inability of this extra NTE to interact with TPR reduces release of MPS1 from kinetochores and decreases sensitivity to displacement by microtubules. Because the TPR domain has an important contribution to MPS1 kinetochore binding, in addition to regulation of the NTE (Nijenhuis et al., 2013), it will be important to define this contribution, as well as the mechanisms by which MPS1 is regulated by both itself and Aurora B.

The metaphase delay observed in MPS1^{2xNTE}-expressing cells is similar to previously tested conditions in which MPS1 was tethered to kinetochores via fusion to the MIS12 protein (Jelluma et al., 2010). Consistently, both situations display elevated levels at kinetochores of SAC components downstream of MPS1 activity. However, MPS1^{2xNTE} appears to promote KNL1-MELT phosphorylation and BUB1 recruitment more efficiently than MAD1 recruitment (Figures 4D, 4E, S4D, and S4E). In addition, although MAD1 kinetochore levels were low on average in MPS1^{2xNTE} metaphase cells, they were quite variable among kinetochores, implying that only a subset of kinetochores was proficient in generating a strong-enough SAC response. MPS1^{2xNTE} may thus expose conditions in which the balance between SAC activating and SAC silencing mechanisms (kinase, phosphatase, and dynein) is near a tipping point. As such, MPS1^{2xNTE} may be a useful tool to examine which SAC silencing events are most sensitive to reductions in MPS1 and how.

Previous work showed that MPS1 interacts with NDC80-C in two regions: the NTE-TPR region interacting with HEC1, and the MR region, interacting with NUF2 (Hiruma et al., 2015; Ji et al., 2015). The affinity of full-length MPS1^{WT} and of MPS1¹⁻³⁷⁷ produced in insect cells (and thus at least partially

phosphorylated) for labeled NDC80-C^{Bonsai} *in vitro* is estimated here as ~400 nM, similar to what has been previously estimated in a different experimental configuration (270 nM) (Hiruma et al., 2015). MPS1^{2xNTE} showed a second binding event with about two orders of magnitude higher affinity (~5 nM), suggesting either the tighter binding of the second NTE compared to the one adjacent to the TPR domain or the presence of a second, unknown binding site. Microtubules inhibit binding of MPS1 to NDC80-C in an at least partly non-competitive manner (Hiruma et al., 2015; Ji et al., 2015). The MPS1^{2xNTE} variant, which is insensitive to the two most prominent regulators of MPS1-NDC80-C interactions (Aurora B and MPS1), is substantially displaced upon microtubule attachments. However, it does not reach the basal levels observed for MPS1^{WT} and is maintained substantially on metaphase kinetochores without noticeable effects on microtubule occupancies. This supports a hypothesis that microtubules cause full dissociation of MPS1 from attached kinetochores by promoting NTE-TPR interactions, in addition to competing with the NTE-NDC80-C interaction, for example, by the kinetochore enrichment of phosphatases that act on the NTE (Hiruma et al., 2015).

This study sheds more light on the complex relationship among MPS1, kinetochores, and microtubules and reveals that regulated intramolecular interactions in MPS1 act alongside the microtubule competition to efficiently displace MPS1 from kinetochores. The layer of regulation that we describe here is therefore important in ensuring smooth mitotic progression and in enabling SAC silencing once stable end-on microtubule attachments have been formed.

STAR★METHODS

Detailed methods are provided in the online version of this paper and include the following:

- KEY RESOURCES TABLE
- CONTACT FOR REAGENT AND RESOURCE SHARING
- EXPERIMENTAL MODEL AND SUBJECT DETAILS
 - Human Cell Lines
 - Bacterial strains and Insect cells
- METHOD DETAILS
 - Isotopically labeled compounds
 - Protein production
 - NMR measurements and backbone assignment
 - Backbone torsion angle restraints calculation
 - NTE-TPR sequence conservation
 - Microscale Thermophoresis and analysis
 - Generation of stable cell lines
 - Plasmids and cloning
 - Knockdown, addback and additional cell treatments
 - Fixed cell immunofluorescence microscopy and image quantification
 - Live cell imaging and movie analysis
 - Fluorescence recovery after photobleaching (FRAP)
 - Immunoblotting
 - Antibodies
- QUANTIFICATION AND STATISTICAL ANALYSIS
- DATA AND SOFTWARE AVAILABILITY

SUPPLEMENTAL INFORMATION

Supplemental Information can be found with this article online at <https://doi.org/10.1016/j.celrep.2019.01.017>.

ACKNOWLEDGMENTS

We thank all Kops and Perrakis lab members for suggestions and discussions. We especially acknowledge Prof. Marcellus Ubbink for providing access to the NMR facility at the Leiden Institute of Chemistry (Leiden University) and for critically discussing initial NMR experiments and data, Wouter Touw for help with the TALOS software, and Marvin Tanenbaum and his group for help with FRAP experiments. This work is part of the Oncode Institute and was funded by grants from the Dutch Cancer Society (KWF/HUBR-2012-5427) and from the Netherlands Organisation for Scientific Research (NWO-Vici 865.12.004). E.C.T. is supported by a postdoctoral fellowship from the Herchel Smith Fund in Cambridge, UK.

AUTHOR CONTRIBUTIONS

S.T.P., A.P., and G.J.P.L.K. conceived the project. Y.H. and S.T.P. performed and analyzed experiments, supervised by A.P. and G.J.P.L.K. E.C.T. performed conservation analysis. S.T.P., A.P., and G.J.P.L.K. wrote the manuscript.

DECLARATION OF INTERESTS

The authors declare no competing interests.

Received: October 22, 2018

Revised: December 13, 2018

Accepted: January 4, 2019

Published: February 19, 2019

REFERENCES

- Araki, Y., Gombos, L., Migueletti, S.P.S., Sivashanmugam, L., Antony, C., and Schiebel, E. (2010). N-terminal regions of Mps1 kinase determine functional bifurcation. *J. Cell Biol.* **189**, 41–56.
- Aravamudan, P., Goldfarb, A.A., and Joglekar, A.P. (2015). The kinetochore encodes a mechanical switch to disrupt spindle assembly checkpoint signaling. *Nat. Cell Biol.* **17**, 868–879.
- Carmena, M., Wheelock, M., Funabiki, H., and Earnshaw, W.C. (2012). The chromosomal passenger complex (CPC): from easy rider to the godfather of mitosis. *Nat. Rev. Mol. Cell Biol.* **13**, 789–803.
- Carpenter, A.E., Jones, T.R., Lamprecht, M.R., Clarke, C., Kang, I.H., Friman, O., Guertin, D.A., Chang, J.H., Lindquist, R.A., Moffat, J., et al. (2006). CellProfiler: image analysis software for identifying and quantifying cell phenotypes. *Genome Biol.* **7**, R100.
- Chao, W.C.H., Kulkarni, K., Zhang, Z., Kong, E.H., and Barford, D. (2012). Structure of the mitotic checkpoint complex. *Nature* **484**, 208–213.
- Ciferri, C., Pasqualato, S., Screpanti, E., Varet, G., Santaguida, S., Dos Reis, G., Maiolica, A., Polka, J., De Luca, J.G., De Wulf, P., et al. (2008). Implications for kinetochore-microtubule attachment from the structure of an engineered Ndc80 complex. *Cell* **133**, 427–439.
- Combes, G., Barysz, H., Garand, C., Gama Braga, L., Alharbi, I., Thebault, P., Murakami, L., Bryne, D.P., Stankovic, S., Eyers, P.A., et al. (2018). Mps1 phosphorylates its N-terminal extension to relieve autoinhibition and activate the spindle assembly checkpoint. *Curr. Biol.* **28**, 872–883.e5.
- Dou, Z., Liu, X., Wang, W., Zhu, T., Wang, X., Xu, L., Abrieu, A., Fu, C., Hill, D.L., and Yao, X. (2015). Dynamic localization of Mps1 kinase to kinetochores is essential for accurate spindle microtubule attachment. *Proc. Natl. Acad. Sci. USA* **112**, E4546–E4555.
- Eddy, S.R. (2011). Accelerated profile HMM searches. *PLoS Comput. Biol.* **7**, e1002195.
- Edelstein, A., Amodaj, N., Hoover, K., Vale, R., and Stuurman, N. (2010). Computer control of microscopes using μ Manager. *Curr. Protoc. Mol. Biol.* **92**, 14.20.1–14.20.17.
- Espert, A., Uluocak, P., Bastos, R.N., Mangat, D., Graab, P., and Gruneberg, U. (2014). PP2A-B56 opposes Mps1 phosphorylation of Knl1 and thereby promotes spindle assembly checkpoint silencing. *J. Cell Biol.* **206**, 833–842.
- Etemad, B., and Kops, G.J.P.L. (2016). Attachment issues: kinetochore transformations and spindle checkpoint silencing. *Curr. Opin. Cell Biol.* **39**, 101–108.
- Eytan, E., Wang, K., Miniowitz-Shemtov, S., Sitry-Shevah, D., Kaisari, S., Yen, T.J., Liu, S.-T., and Hershko, A. (2014). Disassembly of mitotic checkpoint complexes by the joint action of the AAA-ATPase TRIP13 and p31(comet). *Proc. Natl. Acad. Sci. USA* **111**, 12019–12024.
- Faesen, A.C., Thanasoula, M., Maffini, S., Breit, C., Müller, F., van Gerwen, S., Bange, T., and Musacchio, A. (2017). Basis of catalytic assembly of the mitotic checkpoint complex. *Nature* **542**, 498–502.
- Foster, S.A., and Morgan, D.O. (2012). The APC/C subunit Mnd2/Apc15 promotes Cdc20 autoubiquitination and spindle assembly checkpoint inactivation. *Mol. Cell* **47**, 921–932.
- Funabiki, H., and Wynne, D.J. (2013). Making an effective switch at the kinetochore by phosphorylation and dephosphorylation. *Chromosoma* **122**, 135–158.
- Gassmann, R., Holland, A.J., Varma, D., Wan, X., Civril, F., Cleveland, D.W., Oegema, K., Salmon, E.D., and Desai, A. (2010). Removal of Spindly from microtubule-attached kinetochores controls spindle checkpoint silencing in human cells. *Genes Dev.* **24**, 957–971.
- Gorbsky, G.J. (2013). Cohesion fatigue. *Curr. Biol.* **23**, R986–R988.
- Hardwick, K.G., Johnston, R.C., Smith, D.L., and Murray, A.W. (2000). MAD3 encodes a novel component of the spindle checkpoint which interacts with Bub3p, Cdc20p, and Mad2p. *J. Cell Biol.* **148**, 871–882.
- Hewitt, L., Tighe, A., Santaguida, S., White, A.M., Jones, C.D., Musacchio, A., Green, S., and Taylor, S.S. (2010). Sustained Mps1 activity is required in mitosis to recruit O-Mad2 to the Mad1-C-Mad2 core complex. *J. Cell Biol.* **190**, 25–34.
- Hiruma, Y., Sacristan, C., Pachis, S.T., Adamopoulos, A., Kuijt, T., Ubbink, M., von Castelmuir, E., Perrakis, A., and Kops, G.J.P.L. (2015). Cell division cycle. Competition between MPS1 and microtubules at kinetochores regulates spindle checkpoint signaling. *Science* **348**, 1264–1267.
- Hiruma, Y., Koch, A., Hazraty, N., Tsakou, F., Medema, R.H., Joosten, R.P., and Perrakis, A. (2017). Understanding inhibitor resistance in Mps1 kinase through novel biophysical assays and structures. *J. Biol. Chem.* **292**, 14496–14504.
- Howell, B.J., McEwen, B.F., Canman, J.C., Hoffman, D.B., Farrar, E.M., Rieder, C.L., and Salmon, E.D. (2001). Cytoplasmic dynein/dynactin drives kinetochore protein transport to the spindle poles and has a role in mitotic spindle checkpoint inactivation. *J. Cell Biol.* **155**, 1159–1172.
- Howell, B.J., Moree, B., Farrar, E.M., Stewart, S., Fang, G., and Salmon, E.D. (2004). Spindle checkpoint protein dynamics at kinetochores in living cells. *Curr. Biol.* **14**, 953–964.
- Jelluma, N., Brenkman, A.B., McLeod, I., Yates, J.R., 3rd, Cleveland, D.W., Medema, R.H., and Kops, G.J.P.L. (2008a). Chromosomal instability by inefficient Mps1 auto-activation due to a weakened mitotic checkpoint and lagging chromosomes. *PLoS ONE* **3**, e2415.
- Jelluma, N., Brenkman, A.B., van den Broek, N.J.F., Crujisen, C.W.A., van Osch, M.H.J., Lens, S.M.A., Medema, R.H., and Kops, G.J.P.L. (2008b). Mps1 phosphorylates Borealin to control Aurora B activity and chromosome alignment. *Cell* **132**, 233–246.
- Jelluma, N., Dansen, T.B., Slidrecht, T., Kwiatkowski, N.P., and Kops, G.J.P.L. (2010). Release of Mps1 from kinetochores is crucial for timely anaphase onset. *J. Cell Biol.* **191**, 281–290.
- Ji, Z., Gao, H., and Yu, H. (2015). Cell division cycle. Kinetochore attachment sensed by competitive Mps1 and microtubule binding to Ndc80C. *Science* **348**, 1260–1264.

- Ji, Z., Gao, H., Jia, L., Li, B., and Yu, H. (2017). A sequential multi-target Mps1 phosphorylation cascade promotes spindle checkpoint signaling. *eLife* 6, e22513.
- Kang, J., Chen, Y., Zhao, Y., and Yu, H. (2007). Autophosphorylation-dependent activation of human Mps1 is required for the spindle checkpoint. *Proc. Natl. Acad. Sci. USA* 104, 20232–20237.
- Katoh, K., and Standley, D.M. (2013). MAFFT multiple sequence alignment software version 7: improvements in performance and usability. *Mol. Biol. Evol.* 30, 772–780.
- Kemmler, S., Stach, M., Knapp, M., Ortiz, J., Pfannstiel, J., Ruppert, T., and Lechner, J. (2009). Mimicking Ndc80 phosphorylation triggers spindle assembly checkpoint signalling. *EMBO J.* 28, 1099–1110.
- Koch, A., Maia, A., Janssen, A., and Medema, R.H. (2016). Molecular basis underlying resistance to Mps1/TTK inhibitors. *Oncogene* 35, 2518–2528.
- Kops, G.J.P.L., and Shah, J.V. (2012). Connecting up and clearing out: how kinetochore attachment silences the spindle assembly checkpoint. *Chromosoma* 121, 509–525.
- Kruse, T., Zhang, G., Larsen, M.S.Y., Lischetti, T., Streicher, W., Kragh Nielsen, T., Bjørn, S.P., and Nilsson, J. (2013). Direct binding between BubR1 and B56-PP2A phosphatase complexes regulate mitotic progression. *J. Cell Sci.* 126, 1086–1092.
- Kwiatkowski, N., Jelluma, N., Filipakopoulos, P., Soundararajan, M., Manak, M.S., Kwon, M., Choi, H.G., Sim, T., Deveraux, Q.L., Rottmann, S., et al. (2010). Small-molecule kinase inhibitors provide insight into Mps1 cell cycle function. *Nat. Chem. Biol.* 6, 359–368.
- Lan, W., and Cleveland, D.W. (2010). A chemical tool box defines mitotic and interphase roles for Mps1 kinase. *J. Cell Biol.* 190, 21–24.
- London, N., and Biggins, S. (2014a). Signalling dynamics in the spindle checkpoint response. *Nat. Rev. Mol. Cell Biol.* 15, 736–747.
- London, N., and Biggins, S. (2014b). Mad1 kinetochore recruitment by Mps1-mediated phosphorylation of Bub1 signals the spindle checkpoint. *Genes Dev.* 28, 140–152.
- London, N., Ceto, S., Ranish, J.A., and Biggins, S. (2012). Phosphoregulation of Spc105 by Mps1 and PP1 regulates Bub1 localization to kinetochores. *Curr. Biol.* 22, 900–906.
- Maciejowski, J., Drechsler, H., Grundner-Culemann, K., Ballister, E.R., Rodriguez-Rodriguez, J.A., Rodriguez-Bravo, V., Jones, M.J.K., Foley, E., Lampson, M.A., Daub, H., et al. (2017). Mps1 regulates kinetochore-microtubule attachment stability via the ska complex to ensure error-free chromosome segregation. *Dev. Cell* 41, 143–156.
- Mattison, C.P., Old, W.M., Steiner, E., Huneycutt, B.J., Resing, K.A., Ahn, N.G., and Winey, M. (2007). Mps1 activation loop autophosphorylation enhances kinase activity. *J. Biol. Chem.* 282, 30553–30561.
- Maure, J.-F., Kitamura, E., and Tanaka, T.U. (2007). Mps1 kinase promotes sister-kinetochore bi-orientation by a tension-dependent mechanism. *Curr. Biol.* 17, 2175–2182.
- Mische, S., He, Y., Ma, L., Li, M., Serr, M., and Hays, T.S. (2008). Dynein light intermediate chain: an essential subunit that contributes to spindle checkpoint inactivation. *Mol. Biol. Cell* 19, 4918–4929.
- Moura, M., Osswald, M., Leça, N., Barbosa, J., Pereira, A.J., Maiato, H., Sunkel, C.E., and Conde, C. (2017). Protein phosphatase 1 inactivates Mps1 to ensure efficient spindle assembly checkpoint silencing. *eLife* 6, e25366.
- Musacchio, A. (2015). The molecular biology of spindle assembly checkpoint signaling dynamics. *Curr. Biol.* 25, R1002–R1018.
- Nijenhuis, W., von Castelmur, E., Littler, D., De Marco, V., Tromer, E., Vleugel, M., van Osch, M.H.J., Snel, B., Perrakis, A., and Kops, G.J.P.L. (2013). A TPR domain-containing N-terminal module of MPS1 is required for its kinetochore localization by Aurora B. *J. Cell Biol.* 201, 217–231.
- Nijenhuis, W., Vallardi, G., Teixeira, A., Kops, G.J.P.L., and Saurin, A.T. (2014). Negative feedback at kinetochores underlies a responsive spindle checkpoint signal. *Nat. Cell Biol.* 16, 1257–1264.
- Pachis, S.T., and Kops, G.J.P.L. (2018). Leader of the SAC: molecular mechanisms of Mps1/TTK regulation in mitosis. *Open Biol.* 8, 180109.
- Ricke, R.M., and van Deursen, J.M. (2013). Aneuploidy in health, disease, and aging. *J. Cell Biol.* 201, 11–21.
- Rodriguez-Rodriguez, J.-A., Lewis, C., McKinley, K.L., Sikirzhyski, V., Corona, J., Maciejowski, J., Khodjakov, A., Cheeseman, I.M., and Jallepalli, P.V. (2018). Distinct roles of RZZ and Bub1-KNL1 in mitotic checkpoint signaling and kinetochore expansion. *Curr. Biol.* 28, 3422–3429.
- Rosenberg, J.S., Cross, F.R., and Funabiki, H. (2011). KNL1/Spc105 recruits PP1 to silence the spindle assembly checkpoint. *Curr. Biol.* 21, 942–947.
- Sacristan, C., and Kops, G.J.P.L. (2015). Joined at the hip: kinetochores, microtubules, and spindle assembly checkpoint signaling. *Trends Cell Biol.* 25, 21–28.
- Sacristan, C., Ahmad, M.U.D., Keller, J., Fermie, J., Groenewold, V., Tromer, E., Fish, A., Melero, R., Carazo, J.M., Klumperman, J., et al. (2018). Dynamic kinetochore size regulation promotes microtubule capture and chromosome bi-orientation in mitosis. *Nat. Cell Biol.* 20, 800–810.
- Santaguida, S., Vernieri, C., Villa, F., Ciliberto, A., and Musacchio, A. (2011). Evidence that Aurora B is implicated in spindle checkpoint signalling independently of error correction. *EMBO J.* 30, 1508–1519.
- Saurin, A.T., van der Waal, M.S., Medema, R.H., Lens, S.M.A., and Kops, G.J.P.L. (2011). Aurora B potentiates Mps1 activation to ensure rapid checkpoint establishment at the onset of mitosis. *Nat. Commun.* 2, 316.
- Schilder, J., Löhr, F., Schwalbe, H., and Ubbink, M. (2014). The cytochrome c peroxidase and cytochrome c encounter complex: the other side of the story. *FEBS Lett.* 588, 1873–1878.
- Schindelin, J., Arganda-Carreras, I., Frise, E., Kaynig, V., Longair, M., Pietzsch, T., Preibisch, S., Rueden, C., Saalfeld, S., Schmid, B., et al. (2012). Fiji: an open-source platform for biological-image analysis. *Nat. Methods* 9, 676–682.
- Shen, Y., and Bax, A. (2013). Protein backbone and sidechain torsion angles predicted from NMR chemical shifts using artificial neural networks. *J. Biomol. NMR* 56, 227–241.
- Shepherd, L.A., Meadows, J.C., Sochaj, A.M., Lancaster, T.C., Zou, J., Buttrick, G.J., Rappsilber, J., Hardwick, K.G., and Millar, J.B.A. (2012). Phospho-dependent recruitment of Bub1 and Bub3 to Spc7/KNL1 by Mph1 kinase maintains the spindle checkpoint. *Curr. Biol.* 22, 891–899.
- Shrestha, R.L., and Draviam, V.M. (2013). Lateral to end-on conversion of chromosome-microtubule attachment requires kinesins CENP-E and MCAK. *Curr. Biol.* 23, 1514–1526.
- Slidrecht, T., Zhang, C., Shokat, K.M., and Kops, G.J.P.L. (2010). Chemical genetic inhibition of Mps1 in stable human cell lines reveals novel aspects of Mps1 function in mitosis. *PLoS ONE* 5, e10251.
- Stanke, M., Tzvetkova, A., and Morgenstern, B. (2006). AUGUSTUS at EGASP: using EST, protein and genomic alignments for improved gene prediction in the human genome. *Genome Biol.* 7 (Suppl 1), 1–8.
- Stucke, V.M., Silljé, H.H.W., Arnaud, L., and Nigg, E.A. (2002). Human Mps1 kinase is required for the spindle assembly checkpoint but not for centrosome duplication. *EMBO J.* 21, 1723–1732.
- Stucke, V.M., Baumann, C., and Nigg, E.A. (2004). Kinetochore localization and microtubule interaction of the human spindle checkpoint kinase Mps1. *Chromosoma* 113, 1–15.
- Sudakin, V., Chan, G.K.T., and Yen, T.J. (2001). Checkpoint inhibition of the APC/C in HeLa cells is mediated by a complex of BUBR1, BUB3, CDC20, and MAD2. *J. Cell Biol.* 154, 925–936.
- Thebault, P., Chirgadze, D.Y., Dou, Z., Blundell, T.L., Elowe, S., and Bolanos-Garcia, V.M. (2012). Structural and functional insights into the role of the N-terminal Mps1 TPR domain in the SAC (spindle assembly checkpoint). *Biochem. J.* 448, 321–328.
- Tong, K.I., Yamamoto, M., and Tanaka, T. (2008). A simple method for amino acid selective isotope labeling of recombinant proteins in *E. coli*. *J. Biomol. NMR* 42, 59–67.

- Uzunova, K., Dye, B.T., Schutz, H., Ladurner, R., Petzold, G., Toyoda, Y., Jarvis, M.A., Brown, N.G., Poser, I., Novatchkova, M., et al. (2012). APC15 mediates CDC20 autoubiquitylation by APC/C(MCC) and disassembly of the mitotic checkpoint complex. *Nat. Struct. Mol. Biol.* *19*, 1116–1123.
- van Hooff, J.J., Tromer, E., van Wijk, L.M., Snel, B., and Kops, G.J. (2017). Evolutionary dynamics of the kinetochore network in eukaryotes as revealed by comparative genomics. *EMBO Rep.* *18*, 1559–1571.
- Vranken, W.F., Boucher, W., Stevens, T.J., Fogh, R.H., Pajon, A., Llinas, M., Ulrich, E.L., Markley, J.L., Ionides, J., and Laue, E.D. (2005). The CCPN data model for NMR spectroscopy: development of a software pipeline. *Proteins* *59*, 687–696.
- Wang, K., Sturt-Gillespie, B., Hittle, J.C., Macdonald, D., Chan, G.K., Yen, T.J., and Liu, S.-T. (2014). Thyroid hormone receptor interacting protein 13 (TRIP13) AAA-ATPase is a novel mitotic checkpoint-silencing protein. *J. Biol. Chem.* *289*, 23928–23937.
- Westhorpe, F.G., Tighe, A., Lara-Gonzalez, P., and Taylor, S.S. (2011). p31comet-mediated extraction of Mad2 from the MCC promotes efficient mitotic exit. *J. Cell Sci.* *124*, 3905–3916.
- Wheeler, T.J., Clements, J., and Finn, R.D. (2014). Skylign: a tool for creating informative, interactive logos representing sequence alignments and profile hidden Markov models. *BMC Bioinformatics* *15*, 7.
- Yamagishi, Y., Yang, C.-H., Tanno, Y., and Watanabe, Y. (2012). MPS1/Mph1 phosphorylates the kinetochore protein KNL1/Spc7 to recruit SAC components. *Nat. Cell Biol.* *14*, 746–752.
- Ye, Q., Rosenberg, S.C., Moeller, A., Speir, J.A., Su, T.Y., and Corbett, K.D. (2015). TRIP13 is a protein-remodeling AAA+ ATPase that catalyzes MAD2 conformation switching. *eLife* *4*, e07367.
- Zich, J., Sochaj, A.M., Syred, H.M., Milne, L., Cook, A.G., Ohkura, H., Rappsilber, J., and Hardwick, K.G. (2012). Kinase activity of fission yeast Mph1 is required for Mad2 and Mad3 to stably bind the anaphase promoting complex. *Curr. Biol.* *22*, 296–301.

STAR★METHODS

KEY RESOURCES TABLE

REAGENT or RESOURCE	SOURCE	IDENTIFIER
Antibodies		
Guinea pig anti CENP-C	MBL International	Cat# PD030; RRID:AB_10693556
Mouse anti-tubulin	Sigma-Aldrich	Cat# T5168; RRID:AB_477579
Mouse anti-HEC1	Thermo Fisher Scientific	Cat# MA1-23308; RRID:AB_2149871
Rabbit anti-GFP (custom polyclonal serum)		
Mouse anti-GFP	Sigma-Aldrich	Cat# 11814460001; RRID:AB_390913
Mouse anti-MAD1	Millipore	Cat# MABE867;
Rabbit anti-BUB1	Bethyl	Cat# A300-373 A-1; RRID:AB_2065943
Rabbit anti-astrin	Bethyl	Cat# A301-511A; RRID:AB_999598
Mouse anti-MPS1-NT	Millipore	Cat# 05-682; RRID:AB_11214479
Rabbit anti-KNL1-pT180 (custom polyclonal serum)		
Goat anti-guinea pig Alexa Fluor 647	Molecular probes	Cat# A21450; RRID:AB_141882
Goat anti-rabbit Alexa Fluor 488	Molecular probes	Cat# A11034; RRID:AB_142134
Goat anti-rabbit Alexa Fluor 568	Molecular probes	Cat# A11036; RRID:AB_143011
Goat anti-mouse Alexa Fluor 488	Molecular probes	Cat# A11029; RRID:AB_138404
Goat anti-mouse Alexa Fluor 568	Molecular probes	Cat# A11031; RRID:AB_144696
Chemicals, Peptides, and Recombinant Proteins		
¹³ C, ¹⁵ N MPS1 1-239 recombinant protein	This paper	N/A
¹³ C, ¹⁵ N MPS1 62-239 recombinant protein	This paper	N/A
MPS1 recombinant proteins	This paper	N/A
NDC80-C Bonsai (ΔHec1 1-80) recombinant protein	Ciferri et al., 2008	PDB: 2VE7
ZM-447439 (Aurora B inhibitor)	Tocris Bioscience	Cat# 2458
Nocodazole	Sigma-Aldrich	Cat# M1404
MG-132 (proteasome inhibitor)	Sigma-Aldrich	Cat# C2211
Cpd-5 (MPS1 inhibitor)	Koch et al., 2016	N/A
Thymidine	Sigma-Aldrich	Cat# T1895
Doxycycline	Sigma-Aldrich	Cat# D9891
Deposited Data		
MPS1 1-239 backbone assignment	This paper	BMRB: 27641
MPS1 62-239 backbone assignment	This paper	BMRB: 27642
Experimental Models: Cell Lines		
Human: HeLa Flp-In Empty	Gift from S. Taylor lab (University of Manchester)	N/A
HeLa Flp-In LAP-MPS1 WT	Nijenhuis et al., 2013	N/A
HeLa Flp-In LAP-MPS1 Δ60	Nijenhuis et al., 2013	N/A
HeLa Flp-In LAP-MPS1 Δ200	Nijenhuis et al., 2013	N/A
HeLa Flp-In LAP-MPS1 N18P	This study	N/A
HeLa Flp-In LAP-MPS1 N18P-ΔTPR	This study	N/A
HeLa Flp-In LAP-MPS1 2xNTE	This study	N/A
HeLa Flp-In LAP-MPS1 NTE1&2mut	This study	N/A
HeLa Flp-In LAP-MPS1 NTE1mut	This study	N/A
HeLa Flp-In LAP-MPS1 NTE2mut	This study	N/A

(Continued on next page)

Continued

REAGENT or RESOURCE	SOURCE	IDENTIFIER
Oligonucleotides		
siRNA targeting sequence: GAPDH	Dharmacon	D-001830-01-05
siRNA targeting sequence: MPS1 (custom)	Dharmacon	N/A
5'- GACAGAUGAUUCAGUUGUA - 3'	Dharmacon	N/A
Recombinant DNA		
pOG44 Flp-Recombinase expression vector	Invitrogen	Cat# V600520
pcDNA5-LAP-MPS1 WT	Nijenhuis et al., 2013	N/A
pcDNA5-LAP-MPS1 Δ60	Nijenhuis et al., 2013	N/A
pcDNA5-LAP-MPS1 Δ200	Nijenhuis et al., 2013	N/A
pcDNA5-LAP-MPS1 N18P	This study	N/A
pcDNA5-LAP-MPS1 N18P-ΔTPR	This study	N/A
pcDNA5-LAP-MPS1 2xNTE	This study	N/A
pcDNA5-LAP-MPS1 NTE1&2mut	This study	N/A
pcDNA5-LAP-MPS1 NTE1mut	This study	N/A
pcDNA5-LAP-MPS1 NTE2mut	This study	N/A
Software and Algorithms		
TALOS	Shen and Bax, 2013	N/A
Micro-Manager	Edelstein et al., 2010	N/A
Cell Profiler	Carpenter et al., 2006	N/A
CCPN pipeline for NMR data	Vranken et al., 2005	N/A
GraphPad Prism 6	GraphPad Software	N/A
Fiji	Schindelin et al., 2012	N/A
MAAFT	Kato and Standley, 2013	N/A
Skyline	Wheeler et al., 2014	N/A

CONTACT FOR REAGENT AND RESOURCE SHARING

Further information and requests for resources and reagents should be directed to and will be fulfilled by the Lead Contact, Geert Kops (g.kops@hubrecht.eu).

EXPERIMENTAL MODEL AND SUBJECT DETAILS

Human Cell Lines

HeLa Flp-In cells were grown in Dulbecco's modified Eagle medium (DMEM; Sigma D6429) supplemented with 9% tetracycline-free fetal bovine serum (FBS), penicillin-streptomycin (50 μ g ml⁻¹; Sigma P0781) and Ala-Gln (2 mM; Sigma G8541) at 37°C and 5% CO₂.

Bacterial strains and Insect cells

BL21 (DE3) *E. coli* grown at 37°C and Sf9 cells grown at 27°C were used to produce proteins for the biochemical experiments.

METHOD DETAILS

Isotopically labeled compounds

¹⁵NH₄Cl, ¹³C₆-glucose, D₂O and ¹⁵N-asparagine were purchased from CortecNet (Voisins-Le Bretonneux, France)

Protein production

For the proteins used in the NMR experiments, ¹⁵N- and ¹⁵N, ¹³C-enriched minimal media were prepared as described previously ([Schilder et al., 2014](#)). Uniformly isotopically enriched MPS1 samples were produced as following. The plasmids containing the constructs of MPS1 variants were transformed into the BL21(DE3) strain. A single colony was inoculated into 5 mL Lysogeny broth (LB) medium supplemented with 30 μ g mL⁻¹ kanamycin at 37°C for 3 hours. 50 μ L of the pre-culture was transferred into 50 mL of minimal medium and grown at 37°C overnight. 10 mL of the pre-culture was then transferred into 1 L of minimal medium and grown at 37°C

until OD₆₀₀ reached ~0.6. Gene expression was induced with 0.5 mM Isopropyl β -D-1-thiogalactopyranoside (IPTG) and the cultures were allowed to grow at 22°C for 18 hours. Cells were harvested by centrifugation and resuspended in 20 mM KPi, pH 7.5, 1 mM TCEP (buffer A) supplemented with 300 mM KCl, 10 mM imidazole, and 1 mM DNase. Samples were stored at –20°C before proceeding to purification. The resuspended cells were defrosted at room temperature. The sample was lysed by sonication at 50% amplitude for three minutes with Qsonica Sonicator Q700 (Fisher Scientific). The lysate was further disrupted by EmulsiFlex (Avestin). Following centrifugation at 21,000 g for 20 minutes at 4°C, the supernatant was loaded on a HisTrap HP column (GE Healthcare). After extensive washing in buffer A supplemented with 500 mM KCl and 5 mM imidazole, the protein was eluted in the same buffer, but now supplemented with 300 mM imidazole. The samples were diluted three-fold in buffer A with 50 mM KCl and loaded on a HiTrap Heparin HP column (GE Healthcare). After washing with the same buffer, the protein was eluted in buffer A containing 500 mM KCl. The sample was then incubated with 3C protease for affinity tag cleavage at 4°C overnight. The sample was subsequently loaded on a HisTrap HP and HiTrap Heparin column and eluted in buffer A containing 500 mM KCl. The elute was then loaded on a Superdex G75 16/60 HiLoad (GE Healthcare) pre-equilibrated in 20 mM HEPES/NaOH, pH 7.5, 150 mM KCl, 1 mM TCEP and 7% D₂O (buffer B). The protein fractions were pooled together and concentrated. The concentration of the MPS1 samples were determined spectrophotometrically using $\epsilon_{280\text{nm}} = 9.97 \text{ mM}^{-1} \text{ cm}^{-1}$. The purified proteins were aliquoted and stored at –80°C. 15N asparagine labeled –labeled MPS1 samples were produced as a protocol adapted from Tong et al. (Tong et al., 2008).

For the proteins used in the MST experiments, The 1xNTE (WT) and 2xNTE MPS1 constructs (residues 1-377 and 1-808) were cloned into the pFastBac-HT B vector for insect cell expression. Recombinant baculovirus was generated following the manufacturer's instructions (Invitrogen). *Spodoptera frugiperda* (Sf9) insect cells were infected with the baculovirus and allowed to grow for 72 hours at 27°C. Cells were harvested by centrifugation and re-suspended in 50 mL of buffer A supplemented with 150 mM KCl and 10 mM imidazole and one tablet of Pierce Protease Inhibitor Tablets EDTA-free (Thermo Fisher Scientific). Samples were stored at –20°C before proceeding to purification. The re-suspended cells were lysed by sonication for one minute at 50% amplitude in a Qsonica Sonicator Q700 (Fisher Scientific). Following centrifugation at 21,000 g for 20 minutes at 4°C, the supernatant was incubated with Ni²⁺ charged Chelating Sepharose Fast Flow resin (GE Healthcare) for 30 minutes at 4°C. After extensive washing in buffer A supplemented with 500 mM KCl and 5 mM imidazole, the protein was eluted in 15 mL of buffer A supplemented with 50 mM KCl and 300 mM imidazole. The eluent containing MPS1 was subsequently diluted two-fold in buffer A with 50 mM KCl and loaded on a HiTrap Q HP column (GE Healthcare). After washing with the same buffer, the protein was eluted in buffer A containing 400 mM KCl. The sample was then loaded on a Superdex G75 16/60 HiLoad (GE Healthcare) pre-equilibrated in 20 mM HEPES/NaOH, pH 7.5, 150 mM KCl and 1 mM TCEP. The protein fractions were pooled together and concentrated to ~30 μM . The purified protein stored in 50 μL aliquots, flash-frozen by liquid nitrogen and stored at –80°C.

NMR measurements and backbone assignment

The protein concentrations of the ¹³C, ¹⁵N MPS1 #1-239 and ¹³C, ¹⁵N MPS1 #62-239 were 450 μM and 550 μM , respectively in buffer B. All NMR spectra were recorded on a Bruker AVIIIHD 850 spectrometer with a TCI-Z-GRAD cryoprobe at 298 K. The 3D HN(CA)CB, HNCA, HN(CA)CO, HNCO and HN(COCA)CB experiments were acquired for the backbone assignment. The data was processed using Topspin 3.1 (Bruker, Biospin) and spectral assignment and analysis was performed using CCPN analysis 2.1.5. (Vranken et al., 2005).

Sequential assignments of the MPS1 TPR-CTE (residues 62-239) and NTE-TPR-CTE (1-239) domains were performed using combination of HN(CA)CB, HNCA, HN(CA)CO, HNCO and HN(COCA)CB. To refine the assignments, the MPS1 samples were selectively labeled with 15N asparagine. Finally 209 assignments, 87% of assignable residues, were made for the NTE-TPR-CTE construct. It can be noted that most of the peaks that could not be assigned lie in the region of the CTE motif, presumably due to the intermediate exchange dynamics for NMR timescale. Data for backbone assignments (H, N, C α , C β , C) have been deposited to BMRB under codes 27641 (NTE-TPR-CTE) and 27642 (TPR-CTE).

Backbone torsion angle restraints calculation

Phi and psi backbone dihedral angle restraints were predicted by TALOS-N (Shen and Bax, 2013) based on chemical shifts of backbone atoms H, N, C α and C β . Only predictions with a majority consensus in the TALOS-N database and predictions that indicated a dynamic conformation were used for modeling and validation.

NTE-TPR sequence conservation

MPS1 orthologs were defined by searching (Eddy, 2011) the Uniprot database (downloaded on December 6, 2018) and nr (downloaded on December 6, 2018) with inhouse Hidden Markov Models of the TPR and kinase domain, using orthologous group-specific bitscore cut-offs that we previously established (van Hooff et al., 2017). Orthologs with sequence similarities above 98% were discarded and filtered based on relevant phylogenetic positions in the animal tree of life, trying to include as much diversity as possible. MPS1 orthologs for *Lethenteron camtschaticum* and *Petromyzon marinus* were found through an online tblastn search against their respective transcriptomes. The genes were subsequently predicted by the online AUGUST webserver, using pre-trained *Petromyzon marinus*-specific models (Stanke et al., 2006). The resulting set of sequences was aligned to human MPS1 using MAFFT with the option LINSI (Katoh and Standley, 2013). Columns of the alignment that did not contain a residue of the human MPS1 were removed. The sequence logo was build using the skylign webserver with weighted counts and consensus coloring (Wheeler et al., 2014).

Microscale Thermophoresis and analysis

The thermophoresis measurements were performed as previously described (Hiruma et al., 2017) with a slight modification. The DY-547P1 labeled NDC80-C Bonsai (Δ Hec1 1-80) (Ciferri et al., 2008) was used at a final concentration of 50 nM in the ATP buffer (20 mM HEPES, pH 7.4, 100 mM KCl, 1 mM ATP, 4 mM MgCl₂, 1 mM TCEP, 0.05% Tween20). The measurement was performed in duplicates at 20% LED and 40% MST power. The binding curves were fitted with a standard one site model (Equation 1) and two site model (Equation 2) using non-linear regression in GraphPad Prism 6 (GraphPad Software, Inc, USA).

$$Y = \frac{B_{max} * X}{Kd + X} + bg \quad [1]$$

$$Y = \frac{B_{maxHigh} * X}{KdHigh + X} + \frac{B_{maxLow} * X}{KdLow + X} + bg \quad [2]$$

with Y the response; Bmax the maximum response; X the inhibitor concentration; and bg the background response values. An extra sum-of-squares F test was performed with the simpler model being selected unless the p value was under 0.001 to determine which of the two models to select in each case.

Generation of stable cell lines

Plasmids were transfected into Flp-In HeLa cells using Eugene HD (Promega) according to the manufacturer's instructions. To generate stably integrated HeLa Flp-In cell lines, with LAP-tagged genes stably integrated in the FRT site and TetR inducible, pcDNA5 constructs were co-transfected with pOG44 recombinase in a 1:9 ratio and kept in hygromycin (Roche, 10843555001) selection for three weeks.

Plasmids and cloning

pcDNA5-LAP-MPS1 (WT, Δ 60, Δ 200) plasmids were generated in ref 31. All other pcDNA5-LAP MPS1 constructs used in this study were generated from the WT plasmid by standard Gibson assembly protocol of PCR products with primers that either amplify the NTE (to generate the 2xNTE) or that contain the desirable point mutations. pcDNA5-LAP-MPS1^{N18P- Δ TPR} was generated by inserting the N18P mutation with the same strategy but using the pcDNA5-LAP-MPS1 ^{Δ TPR} that was generated in ref 31 as a template.

Knockdown, addback and additional cell treatments

For experiments with knockdown-addback of MPS1, siRNAs for GAPDH (as control, Dharmacon; D-001830-01-05, 20nM) or MPS1 (custom, Dharmacon; 5'-GACAGAUGAUUCAGUUGUA-3', 20nM) were transfected using RNAi Max (Thermo Fisher Scientific) according to manufacturer's instructions. After 16 h of siRNA treatment, cells were arrested in S-phase by addition of thymidine (2 mM; Sigma-Aldrich cat. no. T1895). To induce expression of exogenous LAP-tagged proteins, doxycycline (1 μ g ml⁻¹; Sigma-Aldrich cat. no. D9891) was added 8 hours after the thymidine addition. After 24h of thymidine addition, cells were released and treated with the indicated drugs: ZM-447439 (2 μ M; Tocris Bioscience, cat. no. 2458); Cpd-5 (250 nM; gift from R. H. Medema, Netherlands Cancer Institute); nocodazole (3.3 μ M; Sigma-Aldrich cat. no. M1404). MG-132 (5 mM; cat. no. C2211) was only added 8-9 hours after thymidine release to first allow cells to enter mitosis. Cells were used for further experiments between 8-10 h after thymidine release. For simultaneous knockdown of HEC1 and MPS1, cells were first transfected with 40 nM siHEC1 (custom; Thermo Fisher Scientific; 5'-CCCUGGGUCGUCAGGAA-3'). After 24 hours cells were transfected with a second round of 40 nM siHEC1 and a first round of 20nM siGAPDH or siMPS1. 16 hours later, cells were arrested in S-phase and the protocol continues as above.

Fixed cell immunofluorescence microscopy and image quantification

For immunofluorescence, HeLa Flp-In cells grown on 12 mm coverslip (no. 1.5) were permeabilized for 1 min with warm PEM buffer (100mM Pipes (pH 6.8), 1mM MgCl₂ and 5mM EGTA), followed by fixation for 10 min with 4% PFA in PBS. For analysis of cold-stable microtubules, cells were placed on ice for 15 min prior to pre-extraction and fixation. After fixation, coverslips were washed three times with PBS and blocked with 3% BSA in PBS overnight at 4°C. The next day, primary antibodies diluted in 3% BSA were added to the coverslips and incubated for 2 h at room temperature. Subsequently, cells were washed three times with 0.1% triton in PBS and incubated with secondary antibodies in 3% BSA for another hour at RT. Coverslips were then washed two times with 0.1% Triton in PBS followed by 2 min incubation with DAPI diluted in PBS, followed by two final washes in PBS. Coverslips were then mounted onto glass slides using Prolong Gold antifade. All images were acquired on a deconvolution system (DeltaVision Elite Applied Precision/GE Healthcare) with a \times 100/1.40 NA UPlanSApo objective (Olympus) using SoftWorx 6.0 software (Applied Precision/GE Healthcare). Images were acquired as z stacks at 0.2 μ m intervals and all images of similarly stained experiments were acquired with identical illumination settings. Images were then deconvolved and maximum intensity projections were made using SoftWoRx. Cells were selected based on the mitotic shape of DAPI signal.

For quantification of images, a CellProfiler (Carpenter et al., 2006) pipeline was used to threshold and select all kinetochores and all chromosome areas (excluding kinetochores) using the DAPI and CENP-C. This was used to calculate the relative average kinetochore intensity of various proteins ((kinetochores – chromosome arm intensity (kinetochore localized protein of interest))/(kinetochores – chromosome arm intensity (CENP-C))).

Live cell imaging and movie analysis

For simple live-cell imaging of mitotic timing in various conditions, cells were plated in 24-well plates and DIC filming started 6 hours after thymidine release on a Nikon Ti-E motorized microscope equipped with a Zyla 4.2Mpx sCMOS camera (Andor) and 40 × 1.3 NA objective lens (Nikon). Cells were placed in DMEM without phenol red (Sigma; D1145) supplemented with 9% FBS, penicillin-streptomycin (50 μ g ml⁻¹; Sigma P0781) and Ala-Gln (2 mM; Sigma G8541) and kept at 37°C and 5% CO₂ using a cage incubator and Boldline temperature/CO₂ controller (OKO-Lab). In experiments with DNA visualization, SiR-DNA (Spirochrome, 100nM) was added right after thymidine release and images acquired were comprised of 8 z-slices separated by 2 μ m with the same timing as above. Fluorescence excitation was done using Spectra X LED illumination system (Lumencor) and Chroma-ET filtersets.

Analysis of live-cell imaging experiments was carried out with Fiji software (Schindelin et al., 2012). Time in mitosis for DIC movies was defined as the time between nuclear envelope breakdown (defined as cell rounding) and anaphase-onset or cell flattening. For movies where DNA was visualized, mitosis onset was defined as the first frame where chromatin condensation was observed.

Fluorescence recovery after photobleaching (FRAP)

Cells were grown in 96-square-well glass bottom dishes (Matriplate, Brooks). They were subsequently treated with siMPS1 and expression of MPS1^{WT} or MPS1^{2xNTE} was induced. Cells were arrested in S phase with thymidine and after 24 hours released in nocodazole. 30 minutes before imaging, Cpd-5 was added to inactivate MPS1 and exclude activity dependent changes in turnover and MG132 to prevent cells from exiting mitosis. Mitotic cells were selected and images were acquired using a Yokogawa CSU-X1 spinning disk confocal attached to an inverted Nikon TI microscope with Nikon Perfect Focus system, 100 × NA 1.49 objective, an Andor iXon Ultra 897 EM-CCD camera, and Micro-Manager (Edelstein et al., 2010) and NovaLum software. The EYFP-based LAP tag of LAP-MPS1 was bleached using the 488-nm laser line (Andor FRAP laser box) set to 100%. Areas centered on single kinetochore pairs were bleached once at 100% laser power for 2,000 ms. Fluorescence intensity of the entire cell was acquired for 20 pre-bleach iterations and for 90 iterations after bleach with 100ms intervals.

For each time point, the mean fluorescence intensity was measured in the area that encompassed kinetochore movement and in a similarly sized directly neighboring cytosolic area that was devoid of kinetochores throughout the experiment. Both areas were corrected for background, and the mean fluorescence of the cytosolic area was subtracted from the kinetochore area for each time point ($area_{(KT-cyto)}$). For each measurement, the fluorescence intensity of the $area_{(KT-cyto)}$ in the time point before bleaching was set to 100%, and the measured postbleach $area_{(KT-cyto)}$ signal was normalized to this value. The signal from the bleached kinetochores was corrected for general cell-wise loss in fluorescence by measuring the decline in signal in a non-bleached kinetochore pair. Recovery half-times were determined by nonlinear curve fitting based on a one-phase association followed by a plateau using Prism software (GraphPad Software).

Immunoblotting

Cells were collected by mitotic shake-off and lysed in 50 mM Tris-HCl (pH 7.5), 150 mM NaCl, 2% NP-40, 1 mM EDTA and protease inhibitor cocktail (Roche). Lysates were sonicated and centrifuged for 10' at 20,000 g at 4°C. Supernatants were collected, supplied with Laemmli buffer and boiled for 5 minutes at 96°C. Electrophoresis in SDS-acrylamide gel, transfer to nitrocellulose membranes and immunoblotting were performed using standard protocols. Western blot signals were detected by chemiluminescence using an Amersham Imager 600.

Antibodies

The following primary antibodies were used: CENP-C (polyclonal guinea pig, 1:2,000; MBL, Catalog#: PD 030), α -Tubulin (mouse monoclonal, 1:10,000; Sigma-Aldrich, Catalog#: T5168), HEC1 (mouse monoclonal 9G3, 1:500; Thermo Fisher Scientific, Catalog#: MA1-23308), GFP (custom rabbit polyclonal raised against full-length GFP as antigen, 1:10,000), GFP (mouse monoclonal, 1:1,000; Sigma, Catalog#: 11814460001), MAD1 (mouse monoclonal, 1:1000; Merck Millipore, Catalog#: MABE867), BUB1 (rabbit polyclonal, 1:1,000; Bethyl, Catalog#: A300-373 A-1), Astrin (rabbit polyclonal, 1:1000; Bethyl, Catalog#: A301-511A), MPS1-NT (mouse monoclonal, 1:1000; EMD Millipore, Catalog#: 05-682), KNL1-pT180 (custom rabbit serum against pT180). Secondary antibodies (Invitrogen Molecular Probes, all used at 1:600) were goat anti-guinea pig Alexa Fluor 647 (Catalog#: A21450), goat anti-rabbit Alexa Fluor 488 (Catalog#: A11034), 568 (Catalog#: A11036), and anti-mouse Alexa Fluor 488 (Catalog#: A11029) and 568 (Catalog#: A11031).

QUANTIFICATION AND STATISTICAL ANALYSIS

Results from different experiments were pooled and no difference was observed between different experimental sets. The number of independent experiments and n values are specified in the figure legends. Two-tailed, unpaired t tests or one-way ANOVA followed by Tukey's test were performed to compare either two or multiple experimental groups respectively in immunofluorescence quantifications when experiments were repeated at least 3 times (n refers to number of cells in these experiments). In those cases in which replicates were less than 3, no statistical analysis was performed. Data are presented as mean \pm s.d. All replicates showed similar results and a representative experiment was displayed. Significant differences between the curves fitted to the MST and FRAP data

were inferred by performing extra sum-of-squares F tests. The comparisons most pertinent for the conclusions and p values for all statistical tests performed are annotated in the figures. Graphic representation of data as well as all statistical tests were done with GraphPad Prism 6 for Mac OS.

DATA AND SOFTWARE AVAILABILITY

The accession numbers for backbone assignments (H, N, C α , C β , C) of the NTE-TPR-CTE and TPR-CTE protein fragments reported in this paper in BMRB are 27641 and 27642, respectively.